15th World Congress on Computational Mechanics (WCCM-XV)
8th Asian Pacific Congress on Computational Mechanics (APCOM-VIII)
Virtual Congress: 31 July – 5 August 2022
S. Koshizuka (Ed.)

INTERACTION BETWEEN INDOOR AND OUTDOOR AIR POLLUTION IN NATURAL VENTILATING BUILDING: APPLICATION TO SENSE-CITY URBAN AREA

TSUBASA HAMADA[1], FATIHA CHABI[1], RACHIDA CHAKIR[1], DELPHINE LEJRI[1,2] AND JULIEN WAEYTENS[1]

[1] Université Gustave Eiffel
14 Bd Newton, 77420 Champs-sur-Marne, France
{tsubasa.hamada, fatiha.chabi, rachida.chakir, julien.waeytens}@univ-eiffel.fr
https://www.univ-gustave-eiffel.fr

[2] Université de Lyon
ENTPE, 25 Av François Mitterrand, 69675 Bron, France
delphine.lejri@entpe.fr

Key words: Air Quality, CFD, RANS, Sensitivity Analysis, Sense-City, Full Scale Experiment

Abstract. *As majority of people spend 90% of their time in indoor environment, air quality has become an important scientific field in the last few decades. Indoor air quality is affected by many factors. One of the significant factors is outdoor air pollutions* [1]. *They enter the indoors through ventilation systems or natural ventilation and may stay indoors for a long time due to the airtightness of buildings. The present study especially focuses on nitrogen dioxide (NO2) concentration in a natural ventilating room that comes from outdoor pollutant sources such as vehicle emissions. In the present study, we have performed numerical simulations of a controlled environment in Sense-City urban area* [2]. *Sense-City is a unique full-scale equipment that can reproduce controlled conditions of temperature, humidity, airflow and pollution using an atypical climatic chamber. Reynolds Averaged Navier-Stokes (RANS) simulations have been carried out to calculate indoor and outdoor NO2 concentrations. RANS simulations are performed in two steps: district scale and building scale. Pressure values and pollutant concentrations are extracted from the district scale simulation and applied to the building scale simulation as boundary conditions. As expected, a sensitivity analysis study shows that the NO2 concentration in the building depends mainly on the pollutant concentration at the windows. Once opening windows, indoor pollutant concentration reached the almost same level of that of outdoor within a few minutes. Therefore, the interaction between indoor and outdoor air quality cannot be negligible for indoor air quality. This study can be useful for engineers and for local authorities to understand the importance of considering the interaction of the indoors and outdoors, the potential and limitation of RANS simulation in a natural ventilating. Considering the limitation of the number of sensors for air pollution in real applications, Computational Fluid Dynamics (CFD) is promising to obtain air pollutant distribution cartography. It can also be used as a decision-support tool for relevant urban planning such as the optimal placement of sensors and depolluting systems in urban areas.*

1 INTRODUCTION

As the majority of people spend 90% of their time in indoor environments, its air quality contributes to occupants' health risk, comfort and work efficiency. According to World Health Organization (WHO), poor indoor air quality is responsible for 3.8 million of death every year. Indoor air quality is affected by many factors. One of the significant factors is outdoor air pollution [3,4]. They enter the indoor through ventilation systems and infiltration, and may stay inside for a long time due to the airtightness of buildings which are being improved nowadays.

There are many studies using field measurements or numerical models to assess air quality. Some field measurement campaigns were performed to estimate outdoor pollutant levels e.g. [5]. The relationship between indoor and outdoor air pollutants was also monitored e.g.[6]. However, it is difficult to accurately capture inhomogeneous distributions of pollutant concentration using only a limited number of sensors. Here CFD addresses this issue. Unlike the measurements by commercial sensors, CFD constructs the spatial domain with high resolution of numerical grids, making it possible to visualize the nonuniform airflow and pollutant concentration. Today's development of computational power assists the wide use of CFD for pollutant assessments both indoors e.g.[7] and outdoors e.g.[8]. Nevertheless, few researches consider the interaction between indoor and outdoor air quality in CFD. One of the reasons is that indoor and outdoor air quality are regarded as different scientific fields. However, as mentioned, their interaction is important for the air quality assessment.

The present numerical study demonstrates two kinds of scenarios considering the interaction between indoor and outdoor air quality with RANS simulation in a controlled district Sense-City where atmospheric conditions can be controlled. NO2 source is located on a road to imitate traffic emissions. The simulation is performed in two steps: district scale and building scale, namely decoupling simulation. For the building scale simulation, the boundary conditions (velocity and pollutant concentration) are extracted from the district scale simulation.

2 BRIEF DESCRIPTION OF SENSE-CITY DISTRICT

Sense-City shown in Figure 1 is a unique facility in Université Gustave Eiffel to aim to artificially provide a real and complex urban environment at the real scale. The facility can be used for a variety of studies regarding urban sustainability; energy performance, air and water quality, distribution networks for fluid and water, and so on.

Sense-City has a movable climatic chamber, which surrounds 400m^2 area and 8 m in height. When the climatic chamber is removed into a neighboring area, the real environment is

(a) 

(b) 

Figure 1: Sense-City district: (a) without climatic chamber, (b) within climatic chamber

available. The climatic chamber generates and repeats a specific weather condition according to scientific needs; such as flow velocity, temperature, humidity and sunlight can be controlled. In the Sense-City district which is highly instrumented, there are a concrete building, two small houses, a road, etc. Herein we focus on the pollutant transport from the Sense-City district to an indoor room of the concrete building.

3 CFD SIMULATION OF POLLUTANT DISPERSION AT DISTRICT SCALE

3.1 Governing equation and solver setting

In the first step, a simulation of the district scale was performed for pollutant dispersion. Before the pollutant dispersion simulation, a flow simulation was done by [9] where the flow was averaged over the last 10 min of the 20 min simulation. Based on the average velocity field, the advection-diffusion equation with a volumic pollutant source term is modeled as below:

$$\frac{\partial C}{\partial t} + \bar{\boldsymbol{u}} \cdot \nabla C - \frac{\nu_t}{SC_t} \nabla^2 C = S \tag{1}$$

where $\bar{\boldsymbol{u}}$ is the average velocity, C represents instantaneous concentrations, and S is the pollutant source term, ν_t is the turbulent viscosity, and SC_t is the turbulent Schmidt number which is 0.7 now. The ratio of ν_t to SC_t provides the turbulent diffusion coefficient, making a big difference in the pollutant dispersion behavior. The governing equation was numerically solved with open source software: Freefem++ [10] based on the finite element method. To obtain numerical stability, SUPG method [11,12] was used. Time step was 0.1 s, and the total time step is 3000 steps corresponding to 5 min.

3.2 Computational domain and boundary condition

Figure 2 shows the numerical mock-up of Sense-City with the climatic chamber. Due to the limitation of representing details of geometry, some simplifications were done. In the district scale simulation, all buildings did not have any windows, meaning that all windows were considered closed or walls. Two boundaries were considered for the fan: inlet fan to generate

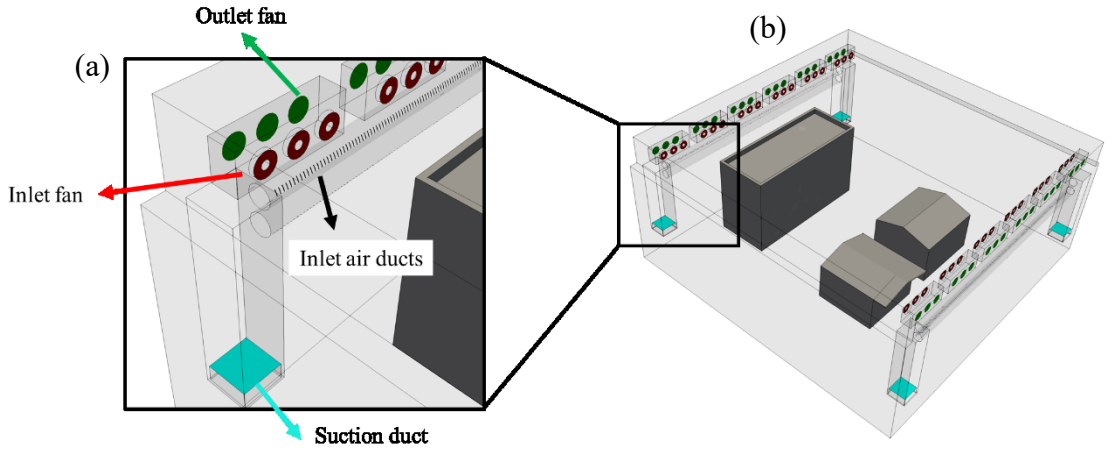

Figure 2: Numerical mock-up of Sense-City district with climatic chamber and its equipment

flow and outlet fan to extract flow. Flow is also extracted by the 4 suction ducts at the corner of Sense-City climatic chamber. More detailed mock-up geometry is available in [9].

In terms of boundary conditions, at the inlet boundary (inlet fans, inlets air ducts) Dirichlet condition for concentration, $C = 0$, was applied. At outlets boundary (outlet fans and suction ducts) and wall surfaces (building, houses, climatic chamber, etc.), Neumann condition for concentration, $\nabla C \cdot n = 0$, was used. Figure 3 represents the position of the pollutant source and streamlines of the average flow. The source was located on a road between the concrete building and the small houses where flow distribution is similar to that of the street canyon. We considered a continuous release of pollutants from box-like source: $0.5 \times 0.5 \times 0.5 = 0.125m^3$ at 1.5 m height. Now we consider the source term S in equation (1) as $S = \gamma f_s(x)$ which is a combination of a strength of emission, γ and a function, $f_s(x)$ expressed by

$$f_s(\mathbf{x}) = \begin{cases} 1 & \text{For } \mathbf{x} \in \Omega_s \\ 0 & elsewhere \end{cases} \quad (2)$$

where Ω_s is the volume of the source. Now γ is set to 1 as a unitary value. Hereafter we consider a simulation with this pollutant source as the elementary solution. The expression, $S = \gamma f_s(x)$, allows us to obtain a desired numerical solution C by multiplying the elementary solution by the desired value (e.g. multiply the elementary solution by 1000 when the strength of source is 1000 $\mu g/m^3/s$).

An unstructured mesh with a local refinement near the source emission was performed using the open-source software SALOME [13] with the automatic mesh generator NETGEN method. After a parametric study of the sensitivity of the results to the grid spacing, a total cell number of about 1,845,707 was retained.

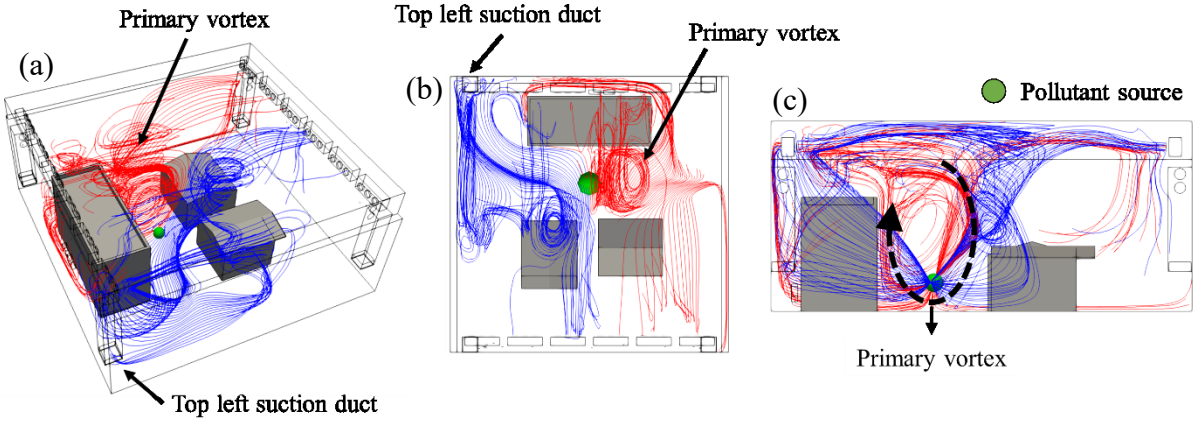

Figure 3: Location of pollutant source and stream line of average flow (both red and blue lines): (a) 3D view, (b) horizontal view, (c) vertical view

3.3 Result: pollutant dispersion at building scale

Figure 4 shows a time evolution of pollutant concentration of the elementary solution on a horizontal plain at z = 1.5m. The pollutants from the source are transported toward the concrete building and then most of the pollutants are sucked into the top left suction duct. Taking into

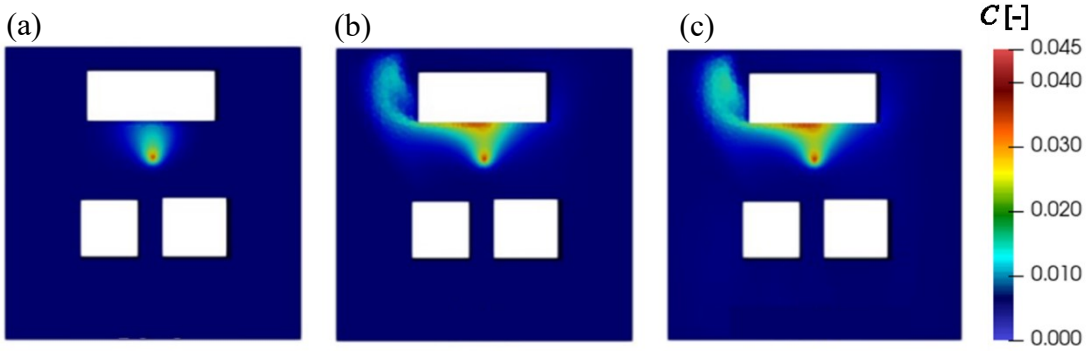

Figure 4: Time evolution of pollutant concentration of the elementary solution: (a) t=5s, (b) t=30s, (c) t=60s

consideration the average flow, the dominant movement toward the left suction duct is caused by the flow of the blue streamlines in Figure 3 (a) and (b). This flow goes down from the inlet fan and directly moves toward the top left suction duct. Red streamlines, on the other hand, move upward along the wall of the concrete building (see Figure 3 (c)), resulting in a big circulation similar to the street canyon's vortex. Therefore, the pollutants are mainly transported upward along the primary vortex (see Figure 5 (a)). From Figure 5 (a), since air pollutants move along the wall, we can note that air pollution can enter the inside concrete building if there is an opening on the wall. In terms of the outside pollutant magnitude from Figure 5, people would be exposed to the poor air quality at the pedestrian level while the pollutant magnitude decreases as it goes upward. However, the pollutant magnitude on the other side of the concrete building is close to zero even at the ground level.

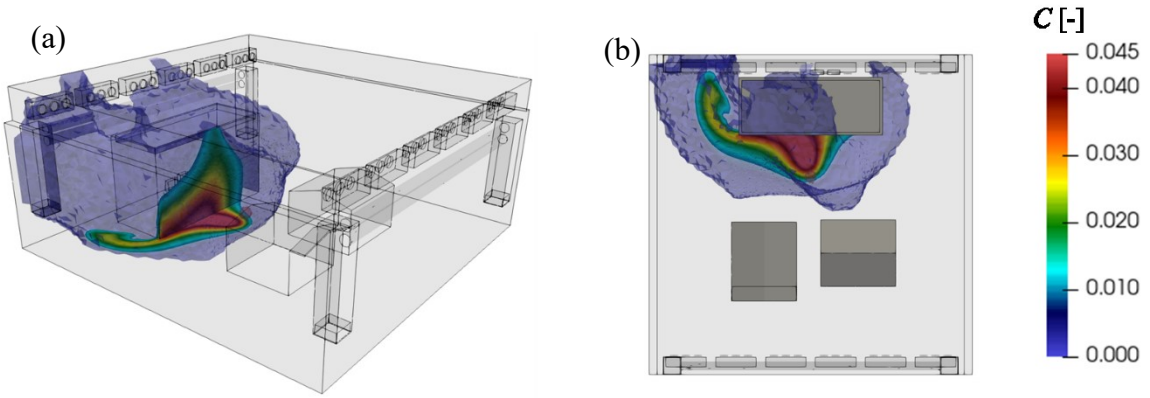

Figure 5: Pollutant concentration at t=30s: (a) 3D view, (b) horizontal view

4 CFD SIMULATION OF FLOW AND POLLUTANT CONCENTRATION AT BUILDING SCALE

4.1 Governing equation and solver setting

We performed both the flow simulation and the pollutant dispersion simulation for the case of the building scale. The solver is Code_Saturne [14] based on finite-volume method for both the flow and pollutant dispersion simulation whereas Freefem++ was used for the pollutant dispersion at the district scale. The governing equation for the flow is Reynolds-Averaged form of incompressible Navier-Stokes equation and continuity equation:

$$\frac{\partial \bar{u}_i}{\partial x_i} = 0 \tag{3}$$

$$\frac{\partial \bar{u}_i}{\partial t} + \bar{u_j}\frac{\partial \bar{u}_i}{\partial x_j} = -\frac{1}{\rho}\frac{\partial \bar{p}}{\partial x_i} + \nu\frac{\partial^2 \bar{u}_i}{\partial x_j x_j} - \frac{\partial \overline{u_i{}' u_j{}'}}{\partial x_j} \tag{4}$$

In the present simulation, the k-ω SST turbulence model [15] was employed, which optimizes the turbulence modeling according to the distance from the wall. The solver setting was identical to [9]. The special terms were discretized with second-order linear upwind (SOLU). The time-advancement scheme was first-order. SIMPLE algorithm is applied for pressure-velocity coupling. Time step was a constant value of 0.1 s. The total simulation period was 30 min. The last 20 min flow was used to obtain an average velocity field with which the advection-diffusion equation was solved. The governing equation was identical to that of the district scale. The same solver setting with the flow simulation was used. The turbulent Schmidt number, SC_t, was 0.7 which was identical to the district scale simulation.

4.2 Computational domain and boundary condition

Figure 6 shows the geometry of the target room located on the first floor of the concrete building including the three desks and a locker. The size of the floor is 9.6 m × 3.6 m and height of 2.3 m. Other small furniture is not mocked-up to simplify the geometry. Two windows are considered inlet and outlet boundary conditions each other in the simulation. One window is open on each side of the wall in the main room (green color shows inlet and red color shows

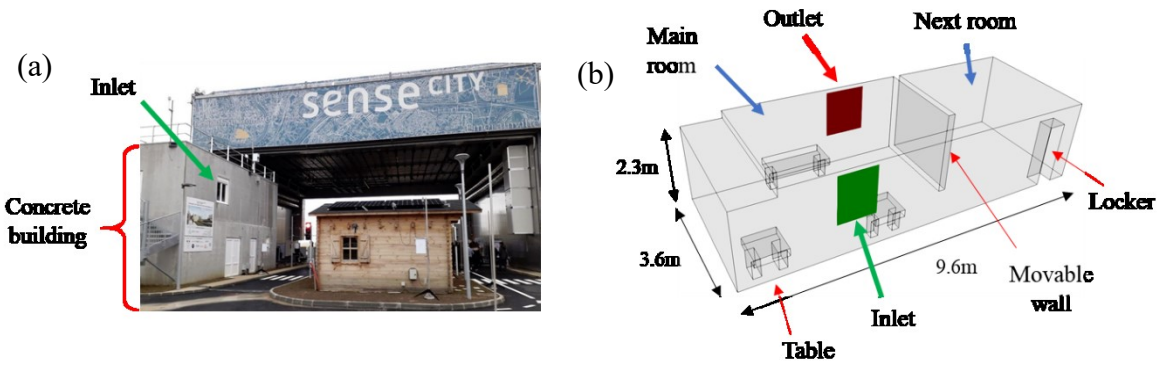

Figure 6: Geometry of indoor building: (a) picture of Sense-City, (b) mock-up indoor building

outlet in Figure 6). The floor is separated by a movable wall, and a 1 m passage is kept open between the main and next room in this case. The distance between the ground and the center of the window is 4.35m.

Figure 7 shows the mesh generated in SALOME. Mesh density varied in each room; refined mesh in the main room and coarse mesh in the next room. To obtain a stable computation, hexa mesh was used only near the inlet and outlet, and tetra mesh fills other spaces.

The boundary conditions for wall, bottom floor, ceiling and furniture employed no-slip conditions. In the present simulation, a window facing the road is regarded as the inlet condition and an opposite side window was the outlet condition. In fact, the flow enters inside from the road side window due to the flow characteristics of Sense-City. At the inlet and outlet conditions, time-averaged pressures that were extracted from the district scale simulation [9] were imposed. Therefore, wind flow inside the room was driven only by pressure difference. At the outlet, zero-gradient condition was imposed for flow and pollutant concentration. For the pollutant concentration, a concentration with a constant magnitude of 1 was imposed at the inlet boundary. Hereafter we regard a numerical solution with these boundary conditions as the elementary solution. Thanks to the linearity of the advection-diffusion equation, the pollutant concentration can be calculated by multiplying the elementary solution by the inlet concentration magnitude obtained from a time-average of the district simulation. The inlet concentration is considered constant in the short-duration simulation.

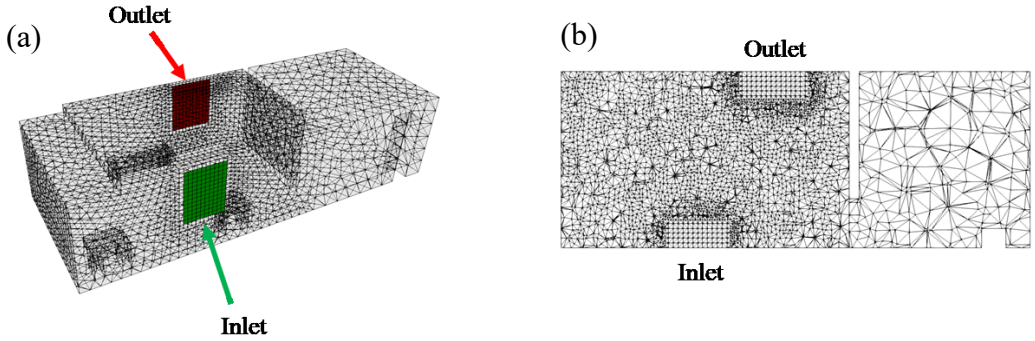

Figure 7: Mesh configuration for indoor building: (a) 3D view, (b) horizontal view

4.3 Mesh convergence study

Before performing the simulation, a mesh convergence study is conducted to obtain a mesh independence solution. Three types of mesh density are investigated. The detail of mesh information is shown in Table 1. Since it is expected that a dominant flow does not appear in the next room, the mesh size is larger than the main room. To avoid numerical instability, the size of hexa mesh near the windows remains. In accordance with German Guideline VDI6019 suggesting a relationship between the number of mesh and volume of a room, the number of adequate mesh is 247,526 in this case. Therefore, we consider the mesh of 255,270 as the intermediate one.

Regarding the average velocity field on the horizontal plane at 1.15 m, as can be seen in Figure 8, it is found that differences between the three cases are not obvious. However, the large-velocity area at the center of the main room (red color regions in Figure 8) elongates as

Table 1: Mesh size

	Main room (m)	Next room (m)	Windows (m)	Total
Coarse	0.22	0.4	0.1	75,699
Intermediate	0.12	0.2	0.1	255,270
Refine	0.1	0.16	0.1	453,005
VDI6019	-	-	-	247,526

the mesh become coarse. In the next room, the center of the circulation is changed each other. Coarse mesh provides a clear circulation in the next room, but this circulation is changed in the other cases. While the coarse mesh does not seem to be affected by the locker, the other two cases show disturbances near the locker leading to the complicated flows. This indicates that the coarse mesh cannot reproduce the flow separation by the locker. Accordingly, the coarse mesh case shows a simpler flow distribution. Given that the coarse mesh is not reliable and the difference between the intermediate and refined is not too big, we decided to choose the intermediate mesh for the following study of the building scale simulation.

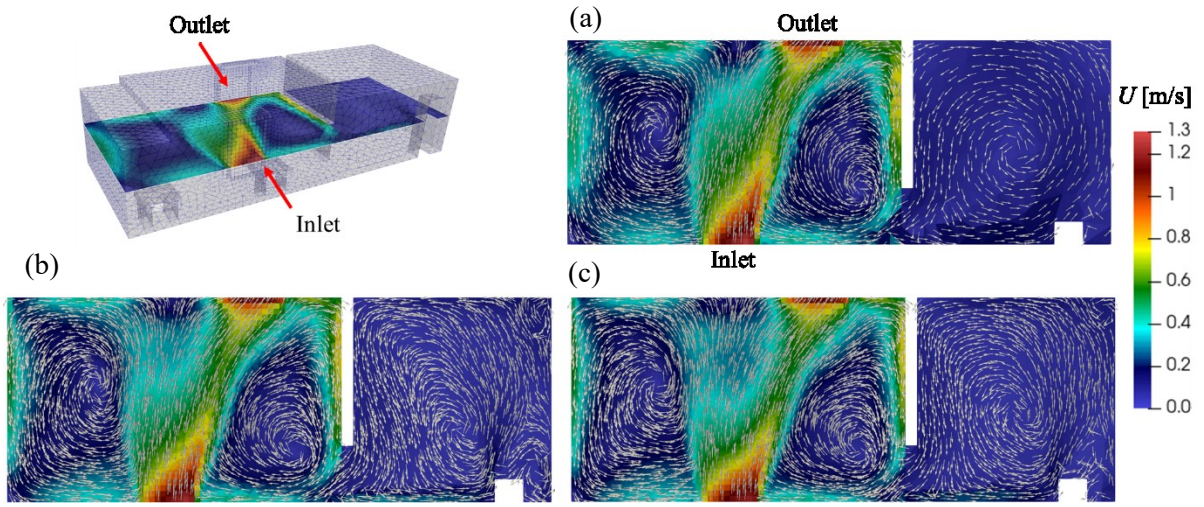

Figure 8: Average velocity field: (a) coarse mesh, (b) intermediate mesh, (c) refine mesh

4.4 Result: flow and pollutant dispersion at building scale

Figure 9 shows the average velocity magnitude and direction calculated from the last 20 min of RANS flow simulation. Flow direction from the inlet window heads toward the outlet window, and then the flow is separated into two directions creating two large 3D circulations in the main room. Accordingly, the center of the room has a lower velocity compared to near the walls. In the next room, one has a very low-velocity flow (i.e. less than 0.3 m/s). Near the movable wall, the flow moves upward from the bottom floor with a magnitude of about 0.7 m/s and turns into the next room through the passage between the rooms.

Along this flow, the pollutants are transported in Figure 10. On the one hand, once the pollutants reach the outlet window, they propagate along the wall. On the other hand, regions

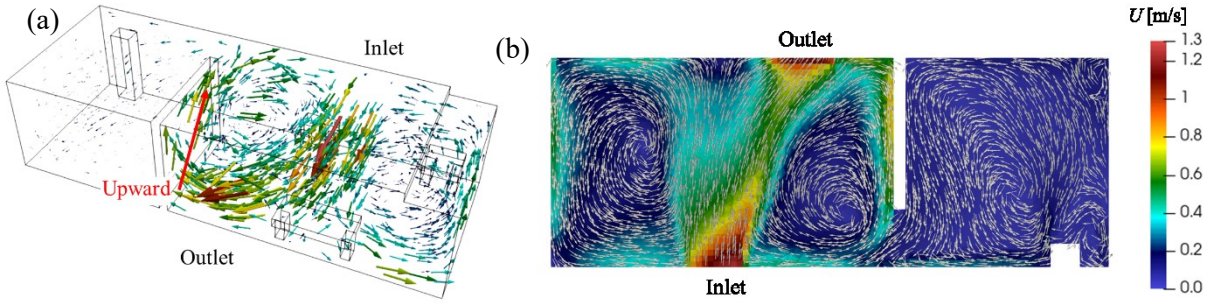

Figure 9: Average velocity field: (a) 3D view, (b) horizontal view

far away from the wall (e.g. the center of the room) are not relatively contaminated at the beginning. Finally, they enter the next room, especially from the top of the passage.

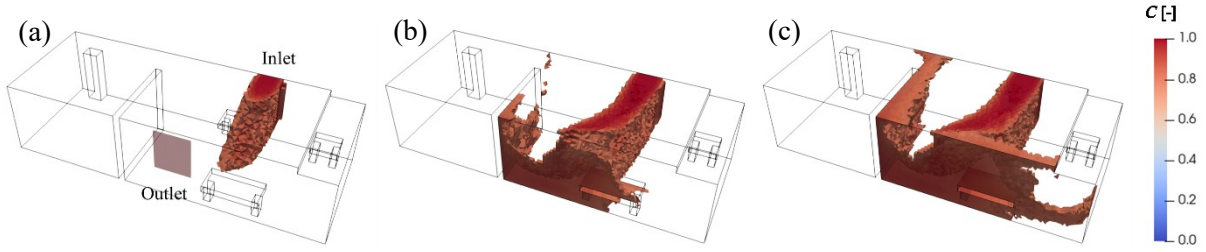

Figure 10: Time evolution of pollutant concentration: (a) t=4s, (b) t=60s, (c) t=100s

Figure 11 (b) shows time evolution of concentration at four probe points (see Figure 11 (a)) to show the sequence of contamination: where it is contaminated firstly, secondly, etc. Point 1 is located in the center of the main room where the main flow occurs, Point 2 near the movable wall with high velocity (i.e. 0.7 m/s), Point 3 in the center of a vortex in the main room, and Point 4 in the next room. Point 1 observes high contamination within a few minutes as this point is in the main flow. Even though the positions of Point 2 and Point 3 are close to each other, their pollutant evolutions show different trends. Point 3 takes more time to reach the high concentration than Point 2. Thus, we can state that air pollutants are propagated from the perimeter to the center of the room gradually. Point 4 indicates a low-speed evolution. This is just the time lag for the pollutant to reach Point 4, and it reaches the same pollutant level of the

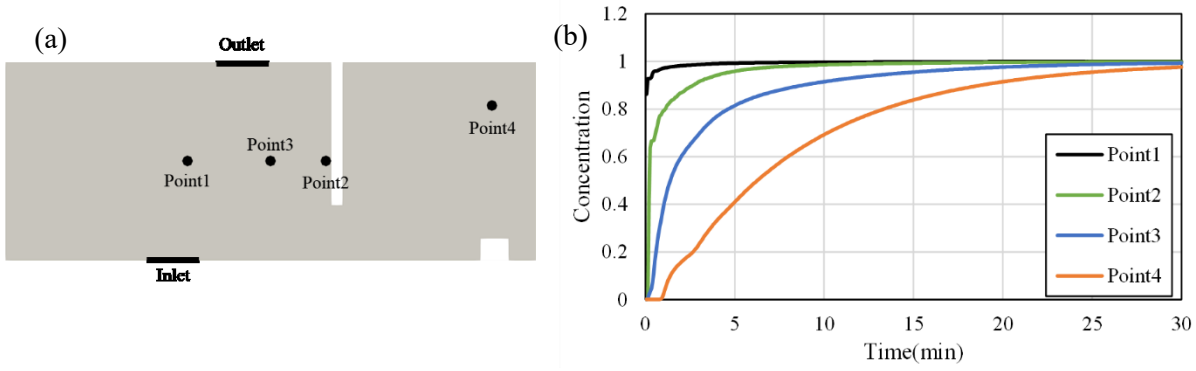

Figure 11: Time history of pollutant concentration on probe points

main room after 30 min. Consequently, hence after 30 min of the window openings, pollutant concentration may be homogeneous in the building room.

4.5 Sensitivity analysis

In order to explore the impact of input variables (pressure difference, Schmidt number and pollutant concentration at the inlet), we performed a numerical sensitivity analysis. Simulations with 10% increase and decrease of pressure difference and Schmidt number were conducted. To evaluate the sensitivity, we consider a non-dimensional indicator of pollutant level I_{dif} on the first 15 min calculated by

$$I_{dif} = \frac{I_i - I_{ref}}{I_{ref}}, \qquad I_{ref} = \frac{1}{15min}\int_0^{15min} C_{ref}\,dt\,, \qquad I_i = \frac{1}{15min}\int_0^{15min} C_i dt \tag{5}$$

where "C_{ref}" represents a reference concentration obtained considering Schmid number SC_t is 0.7, pressure difference between inlet and outlet is 0.633 Ps and inlet concentration magnitude is 1.0. "C_i" represents a numerical concentration where a model parameter has been changed to 10 % compared to its reference value. For instance, "*Pre_min*" indicates a case with a pressure difference of 10% decrease, "*Sch_plus*" shows a case with Schmid number of 10 % increase, and "*Pre_min-Sch_plus*" shows a case combining both above conditions.

Table 1 shows the result of the sensitivity analysis in terms of the pressure difference and Schmidt number on the three probe points. For the impact of the inlet pollutant concentration, thanks to the linearity of the advection-diffusion equation, it is easy to estimate its impact without simulations. Namely ±10 % modification of pollutant concentration at the inlet window will lead to ±10 % variation of the indicator. Point 1 is not sensitive to the change of the pressure difference and Schmidt number. This can be attributed to the short time duration before reaching the high pollutant concentration even with the changed input variables. For Point 3 and Point 4, it is found that the pressure difference has a relatively large impact compared to Schmidt number. However, recalling that the change of ±10 % of the inlet pollutant concentration gives $I_{dif} = \pm 10\%$, the inlet pollutant is the most influential parameter. Therefore, to obtain an accurate prediction of the pollutant level in the room, one needs to previously know the pollutant concentration at the inlet opening from prior simulations or measurements.

Table 2: Indicator of numerical sensitivity analysis: I_{dif}, I_{ref},I_i

	Point 1		Point 3		Point 4	
	I_{ref} = 1.485		I_{ref} = 1.194		I_{ref} = 0.768	
	I_i	I_{dif} (%)	I_i	I_{dif} (%)	I_i	I_{dif} (%)
Pre_min	1.489	0.29	1.145	4.12	0.797	3.75
Pre_plus	1.479	0.39	1.226	2.65	0.761	0.87
Sch_min	1.478	0.48	1.217	1.86	0.776	1.01
Sch_plus	1.487	0.11	1.189	0.42	0.772	0.56
Pre_min-Sch_min	1.489	0.26	1.174	1.68	0.730	4.95
Pre_min-Sch_plus	1.492	0.45	1.170	1.99	0.733	4.57
Pre_plus-Sch_min	1.481	0.28	1.242	4.00	0.716	6.74
Pre_plus-Sch_plus	1.485	0.03	1.235	3.4	0.721	6.10

5 CONCLUSIONS AND FUTURE PERSPECTIVE

In the present study, the numerical simulations for flow and pollutant dispersion in Sense-City were performed at both the district and building scales separately to study the interaction between indoor and outdoor pollutants. Then, in the sensitivity analysis, we investigated which kind of input variables in the simulations are influential on the pollutant concentration in the room. As a result, the following knowledge is obtained:

- Pollutants emitted from the source on a road are transported along the flow and upward along with the building wall, and finally they reach a height of a window on the 1st floor. It can be mentioned that outdoor air pollution affects indoor air quality and it largely depends on the airflow direction and distribution. Thus, it is important to take the dominant flow direction and urban geometry into account when considering adequate actions plans reduce the individual human exposures.

- Pollutants entered the room from the inlet window spread from the perimeter of the room to the center of the room. Even in a small indoor area, the air quality can be inhomogeneous in the first 15 min of the simulation. Therefore, it should be noted that opening windows does not always result in good indoor air quality and people should consider when adequate action plans should be implemented (e.g. opening windows).

- As the indoor pollutant concentration in the simulation is sensitive to the pollutant magnitude at the inlet window, it is crucial for an accurate simulation to get an accurate pollutant magnitude at inlets or pollutant sources from outdoor simulations, experiments and field measurements in advance.

This numerical study will be used to design an experiment in Sense-City (e.g. to know where should be monitored by sensors) and compared with the experiment for validation. Then cartography for air quality in Sense-City will be made. Based on the cartography, we will propose optical placements of depolluting systems using CFD results and an inverse method for Sense-City district. This series of methodology will be extended to a real urban area, Paris, in the future.

REFERENCES

[1] D.Y.C. Leung, Outdoor-indoor air pollution in urban environment: Challenges and opportunity, Front. Environ. Sci. 2 (2015) 1–7. https://doi.org/10.3389/fenvs.2014.00069.

[2] D. François, L. Bérengère, H.V.D. T. Bourouina, Fr´ed´eric Bourquin, Costel-Sorin COJOCARU, Enric Robine, The Sense-City project, XVIIIth Symp. Vib. Shock. Noise. (2012).

[3] E. Rijnders, N.A.H. Janssen, P.H.N. van Vliet, B. Brunekreef, Personal and outdoor nitrogen dioxide concentrations in relation to degree of urbanization and traffic density, Environ. Health Perspect. 109 (2001) 411–417. https://doi.org/10.1289/ehp.01109s3411.

[4] P.H. Fischer, G. Hoek, H. Van Reeuwijk, D.J. Briggs, E. Lebret, J.H. Van Wijnen, S. Kingham, P.E. Elliott, Traffic-related differences in indoor and outdoor concentrations of particles and volatile organic compounds in Amsterdam, Atmos. Environ. 34 (2000) 3713–3722. https://doi.org/10.1016/S1352-2310(00)00067-4.

[5] L. Wang, J. Wang, X. Tan, C. Fang, Analysis of NOx pollution characteristics in the atmospheric environment in Changchun city, Atmosphere (Basel). 11 (2020). https://doi.org/10.3390/ATMOS11010030.

[6] P. Blondeau, V. Iordache, O. Poupard, D. Genin, F. Allard, Relationship between indoor and outdoor air quality in eight French schools, Indoor Air. 15 (2005) 2–12. https://doi.org/10.1111/j.1600-0668.2004.00263.x.

[7] L. Yang, M. Ye, B.J. he, CFD simulation research on residential indoor air quality, Sci. Total Environ. 472 (2014)

1137–1144. https://doi.org/10.1016/j.scitotenv.2013.11.118.
[8] J.L. Santiago, R. Borge, F. Martin, D. de la Paz, A. Martilli, J. Lumbreras, B. Sanchez, Evaluation of a CFD-based approach to estimate pollutant distribution within a real urban canopy by means of passive samplers, Sci. Total Environ. 576 (2017) 46–58. https://doi.org/10.1016/j.scitotenv.2016.09.234.
[9] B. Streichenberger, R. Chakir, B. Jouy, J. Waeytens, Simulation and Validation of CFD turbulent airflow at pedestrian level using 3D ultrasonic anemometer in the controlled urban area “Sense-City,” J. Wind Eng. Ind. Aerodyn. 219 (2021) 104801. https://doi.org/10.1016/j.jweia.2021.104801.
[10] F. Hecht, FreeFem++ users’ guide, (2012). http://www.freefem.org/ff++.
[11] Thomas J.R.Hughes, Mallet, Michel, Akira Mizukami, A new finite element formulation for computational fluid dynamics: II. Beyond SUPG, Comput. Methods Appl. Mech. Eng. 54 (1986) 341–355.
[12] L.P. Franca, S.L. Frey, T.J.R. Hughes, Stabilized finite element methods: I. Application to the advective-diffusive model, Comput. Methods Appl. Mech. Eng. 95 (1992) 253–276. https://doi.org/10.1016/0045-7825(92)90143-8.
[13] SALOME, Salome: Pre- and Post-Processing Platform for Numerical Simulation, (n.d.). www.salome-platform.org.
[14] F. Archambeau, N. M\’{e}chitoua, M. Sakiz, Code Saturne: A Finite Volume Code for Turbulent flows - Industrial Applications, Int. J. Finite Vol. 1 (2004).
[15] D.C. Wilcox, Formulation of the k-ω turbulence model revisited, AIAA J. 46 (2008) 2823–2838. https://doi.org/10.2514/1.36541.